nature communications

Article

https://doi.org/10.1038/s41467-025-67693-6

Superadiabatic topological pumping on photonic chips

Received: 30 June 2025

Accepted: 5 December 2025

Published online: 29 December 2025

Check for updates

Jin-Lei Wu[1,7], Kai-Heng Xiao[2,7], Xiang Ni[3,7], Jin-Kang Guo[1], Xu-Lin Zhang[2], Qi-Dai Chen[2], Yan Wang[4], Ze-Zheng Li[5], Shi-Lei Su[1,6] ✉, Zhen-Nan Tian[2] ✉ & Hong-Bo Sun[2,5] ✉

Adiabatic topological pumping offers a robust mechanism for light transport in integrated photonics, enabling the development of efficient on-chip photonic devices. However, its practical implementations face significant challenges in maintaining both high transport efficiency and scalability due to slow adiabatic modulation requirements, and existing acceleration strategies fall short in achieving substantial device miniaturization. Here, we develop a gap-mode strategy for constructing shortcut to topological pumping, and experimentally demonstrate a superadiabatic paradigm through iterative adiabatic transformations in an on-chip photonic platform. Our approach achieves a 20-fold footprint reduction compared to conventional adiabatic pumping and a 50% size reduction relative to optimized Landau-Zener (as well as recently reported quantum metric and adiabatic infimum) implementations. The device operates over a remarkable bandwidth of 650–920 nm while facilitating scalable waveguide integration. This methodology establishes a framework for realizing high-efficiency topological photonic transport with tailored coupling configurations, paving the way for ultra-compact photonic integrated circuits.

Topological photonics has revolutionized on-chip light manipulation by taking advantage of topological invariance and thus achieving extraordinary control over robust light propagation[1–5]. While static topological insulators have been the focus of early research, dynamic topological pumping, enabled by parameter modulation, has recently emerged as a versatile platform for achieving reconfigurable photonic transport with intrinsic disorder resilience[6–13]. This paradigm offers significant advantages for integrated photonics by facilitating efficient, broadband photon steering between spatially isolated components with robust performance[14–17]. However, practical implementations face a critical constraint: the strict adiabaticity requirements of conventional topological pumping demand low modulation gradients, fundamentally limiting device miniaturization and scalability in integrated photonic systems[18–20].

Various strategies have been explored to overcome this fundamental limitation[21–34]. Despite these advances, existing approaches either rely on adiabatic operation[21–27], compromise topological protection for faster operation[28–30], or lack practical feasibility in integrated photonic platforms[31–34]. Several representative strategies highlight tradeoff between pumping velocity and topological robustness. The Landau-Zener (LZ) approach[21], as well as recently reported quantum metric[26] and adiabatic infimum[27], exploits accelerated conversion between edge states while preserving topological protection. However, its performance hinges on adiabatically suppressed gap-mode transitions, which inherently imposes a upper speed limit. In

[1]School of Physics, Zhengzhou University, Zhengzhou, China. [2]State Key Laboratory of Integrated Optoelectronics, JLU Region, College of Electronic Science and Engineering, Jilin University, Changchun, China. [3]School of Physics, Central South University, Changsha, China. [4]School of Electronics and Information, Zhengzhou University of Light Industry, Zhengzhou, China. [5]State Key Laboratory of Precision Measurement Technology and Instruments, Department of Precision Instrument, Tsinghua University, Beijing, China. [6]Institute of Quantum Science and Technology, Yanbian University, Yanji, Jilin, China. [7]These authors contributed equally: Jin-Lei Wu, Kai-Heng Xiao, Xiang Ni. ✉e-mail: slsu@zzu.edu.cn; zhennan_tian@jlu.edu.cn; hbsun@tsinghua.edu.cn

contrast, Rabi-flopping schemes utilize resonant gap-mode transitions to enable nonadiabatic pumping[28–30], but this gain in speed comes at the cost of topological protection. Strategies based on shortcuts to adiabaticity (STA)[35] offer a powerful paradigm for accelerating adiabatic processes, providing not just a single shortcut but an entire family of accelerated paths connecting the same initial and final states. However, many theoretically proposed STA protocols, often relying on conventional counterdiabatic (CD) driving with next-nearest-neighbor (NNN) or imaginary couplings, remain experimentally inaccessible[31–34]. A key challenge, therefore, is to design shortcuts that are both fast and fully compatible with the native control parameters of the platform.

In this work, we develop a strategy for constructing shortcut to topological pumping by incorporating CD driving into the gap-mode Hamiltonian, and demonstrate a superadiabatic (SUAD) topological pumping scheme that enables high-fidelity, ultra-compact transport in photonic lattices. The shortcut engineering between topologically protected gap modes avoids the need for NNN CD driving. Moreover, the SUAD framework enables experimentally accessible STA in photonic waveguide arrays, relying solely on real parameters natively available in integrated platforms. Using femtosecond laser direct-written waveguide arrays, we experimentally demonstrate SUAD topological pumping with breakthrough performance: a 20-fold smaller footprint than conventional adiabatic pumping, and a 50% greater compactness than the LZ approach as well as quantum metric[26] and adiabatic infimum[27]. The system is predicted to achieve > 0.95 pumping fidelity across a 270 nm bandwidth (wavelength: 650–920 nm), and supports scalable port multiplexing, outperforming state-of-the-art coherent-tunneling adiabatic passage techniques[23,24]. By eliminating the need for slow adiabatic modulation, this work demonstrates that feasible shortcuts can be systematically engineered by aligning theoretical design with physical constraints, and thus paves the way for high-density topological photonics with customizable coupling architectures, opening new frontiers in photonic integration.

Results

System under investigation

Our SUAD topological pumping scheme can apply broadly to systems with two or more topologically protected gap modes, offering a versatile platform for engineering diverse topological transport phenomena. To illustrate its principles, we initiate our investigation with the renowned dimerized Su-Schrieffer-Heeger (SSH) model (Fig. 1a, top right). The photonic waveguides (quantity is N) forming the SSH model (Fig. 1a, bottom left) were fabricated in a boroaluminosilicate glass using femtosecond laser direct writing techniques[10,36] (Methods). The fabricated sample (e.g., 20 waveguides in Fig. 1a, top left) features a single x-polarized mode at 808 nm with ~7 μm × 5 μm cross-sections. This waveguide array system with the length L (maximum 75 mm for our chips) is restricted to nearest-neighbor couplings. The coupling strength c_1 and the propagation constant β_2 are spatially modulated in the z-direction, while c_2 and β_1 remain invariant.

Given that the system adheres to the paraxial approximation in a tight-binding model, the state vector $|\Psi(z)\rangle = \sum_n^N \gamma_n(z)|n\rangle$ of the system along the z axis (γ_n represents the complex probability amplitude of basis vector $|n\rangle$ on the n-th waveguide, $\sum_n^N |\gamma_n(z)|^2 = 1$) is governed by the Schrödinger-like coupled-mode equation (CME) $\hat{H}(z)|\Psi(z)\rangle = -\mathrm{i}\partial_z|\Psi(z)\rangle$. The Hamiltonian is

$$\hat{H}(z) = \sum_{j=1}^{N/2}\left[\beta_1|2j-1\rangle\langle 2j-1| + \beta_2(z)|2j\rangle\langle 2j|\right] + \left[c_1(z)|2j-1\rangle\langle 2j| + \sum_{j=1}^{N/2-1} c_2|2j\rangle\langle 2j+1| + \mathrm{h.c.}\right], \quad (1)$$

where $c_1(z)$ (c_2) is the coupling coefficient between the $2j$-th and the $(2j-1)$-th [$(2j+1)$-th] waveguides, and β_1 [$\beta_2(z)$] is the propagation constant of the x-polarized mode in the $(2j-1)$-th ($2j$-th) waveguide. The system is considered to be prepared in the topologically nontrivial

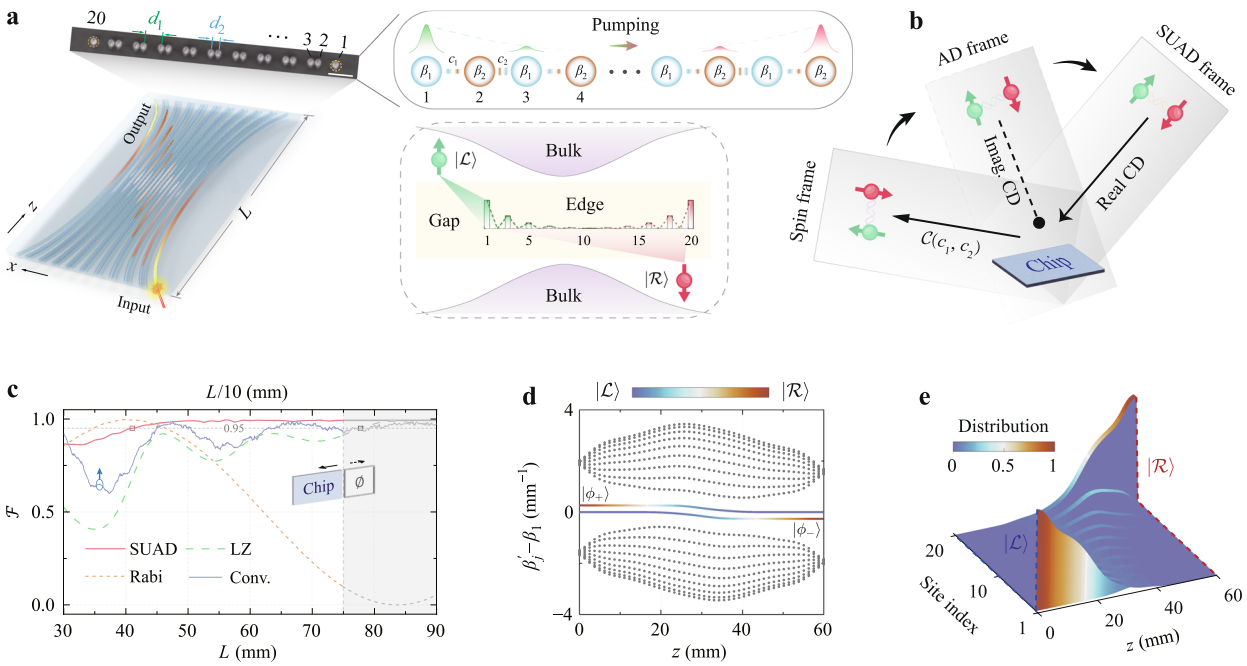

Fig. 1 | Illustration of SUAD topological pumping in modulated photonic waveguides. a Bottom-left panel: schematic of a spatially modulated SSH lattice of photonic waveguides fabricated inside a glass; Top-left panel: photograph of the fabricated sample of waveguides at the output facet (scale bar: 20 μm); Top-right panel: schematic of SSH lattice with finite sites; Bottom-right panel: spectrum schematic for illustrating two gap-protected modes occupying edges of SSH lattice. **b** Schematic relation between on-chip topological pumping and a specified interaction picture of gap-mode pseudospin. AD adiabatic, CD counterdiabatic. **c** Fidelity comparison among four topological pumping schemes in 20 waveguides with varying sample lengths, where the length value in the conventional adiabatic case (Conv.) is divided by ten. **d** Instantaneous propagation constants of eigenmodes relative to β_1. The edge modes in the gap are hybridized into $|\phi_\pm\rangle$. **e** Instantaneous distribution of excitation on each waveguide along SUAD path $|\Phi_-(z)\rangle$. Data in **c**, **d**, **e** are obtained based on the full Hamiltonian $\hat{H}(z)$.

phase $c_1(z) < c_2$ (More strictly $|\Delta\beta(t)/2| < |c_2 - c_1(t)|$; See Supplementary Note 1 for calculation of geometric phases). For a finite number N of waveguides, there exist two gap modes at the edges of system (Fig. 1a, bottom right), respectively

$$|\mathcal{L}\rangle = \mathcal{N}\sum_{j}^{N/2}\chi^{j}|2j-1\rangle,\ |\mathcal{R}\rangle = \mathcal{N}\sum_{j}^{N/2}\chi^{N/2-j}|2j\rangle. \tag{2}$$

$\mathcal{N} = \sqrt{(1-\chi^2)/(1-\chi^N)}$ is the normalization factor with $\chi = -c_1/c_2$. Under the topologically nontrivial phase, the edge modes are protected by the energy gap, and the system is reduced to an effective gap-mode version whose Hamiltonian reads[21,29,37]

$$\widehat{H}_{\text{eff}} = \mathcal{C}(z)\widehat{\sigma}_x - [\Delta\beta(z)/2]\widehat{\sigma}_z. \tag{3}$$

$\widehat{\sigma}_x = |\mathcal{L}\rangle\langle\mathcal{R}| + |\mathcal{R}\rangle\langle\mathcal{L}|$ and $\widehat{\sigma}_z = |\mathcal{L}\rangle\langle\mathcal{L}| - |\mathcal{R}\rangle\langle\mathcal{R}|$ are Pauli operators of the pseudospin formed by two gap modes. $\mathcal{C}(z)$ and $\Delta\beta(z)$ are the effective coupling coefficient and the propagation constant difference between two gap modes, respectively (See Methods for derivation).

Pumping engineering in SUAD picture

CD drivings, which cancel nonadiabatic leakages along the adiabatic reference path, are crucial for implementing shortcuts to adiabatic state transfer[35]. However, in conventional multi-site systems, CD driving protocols often employ NNN and imaginary couplings, posing significant challenges for practical implementation[31–34]. In contrast, the gap-mode Hamiltonian in our system offers a unique advantage for realizing CD driving protocols by inherently eliminating the requirement for NNN couplings. Typically, the CD driving is analyzed in the adiabatic framework, where the gap-mode Hamiltonian is expressed in the interaction picture (Methods)

$$\widehat{H}_{\text{AD}}(z) = \Omega(z)\sum_{l=\pm} l|\phi_l\rangle\langle\phi_l| - \mathrm{i}\partial_z\theta(z)(|\phi_+\rangle\langle\phi_-| - |\phi_-\rangle\langle\phi_+|)/2, \tag{4}$$

and $|\phi_-(z)\rangle = \cos\frac{\theta(z)}{2}|\mathcal{L}\rangle - \sin\frac{\theta(z)}{2}|\mathcal{R}\rangle$ with energies $\pm\Omega(z) \equiv \pm\sqrt{\mathcal{C}(z)^2 + \Delta\beta(z)^2}/4$. The mixed angle $\theta(z) = \arccos[\Delta\beta(z)/2\Omega(z)]$ governs the edge-mode composition of the eigenstate. Nonetheless, in this framework, the CD driving removing nonadiabatic leakages (the second term in $\widehat{H}_{\text{AD}}$) needs imaginary couplings between waveguides (AD frame in Fig. 1b), which presents substantial challenges for standard implementation on photonic platforms.

To realize experimentally feasible CD driving with purely real waveguide couplings, we intend to introduce a dressed-state representation through strategic frame transformations[38–40]. Instead of working in the conventional adiabatic frame, we use the second-order adiabatic iteration to construct SUAD modes (eigenstates of $\widehat{H}_{\text{AD}}$)[41,42]

$$|\Phi_\pm(z)\rangle = \sin\frac{\Theta(z)}{2}|\phi_\mp\rangle - \mathrm{i}\cos\frac{\Theta(z)}{2}|\phi_\pm\rangle, \tag{5}$$

with $\Theta(z) = \arcsin[\partial_z\theta(z)/2\Omega'(z)]$, corresponding to energies $\pm\Omega'(z) \equiv \pm\sqrt{\Omega(z)^2 + \partial_z\theta(z)^2}/4$. In SUAD frame, the Hamiltonian becomes

$$\widehat{H}_{\text{SUAD}}(z) = \Omega'(z)\sum_{l=\pm} l|\Phi_l\rangle\langle\Phi_l| - \partial_z\Theta(z)(|\Phi_+\rangle\langle\Phi_-| + |\Phi_-\rangle\langle\Phi_+|)/2. \tag{6}$$

Correspondingly, the SUAD CD driving term is described by a purely real gap-mode coupling operator $\widehat{h}_{\text{CD}} = \sin\theta(z)\partial_z\Theta(z)\times(|L\rangle\langle L| - |R\rangle\langle R|)/2 + \cos\theta(z)\partial_z\Theta(z)(|L\rangle\langle R| + |R\rangle\langle L|)/2$ (SUAD frame in Fig. 1b). Combining $\widehat{H}_{\text{eff}}$ with $\widehat{h}_{\text{CD}}$ yields modified effective modulation parameters

$$\begin{aligned}\mathcal{C}'(z) &= \Omega(z)\sin\theta(z) + \partial_z\Theta(z)\cos\theta(z)/2,\\ \Delta\beta'(z) &= 2\Omega(z)\cos\theta(z) - \partial_z\Theta(z)\sin\theta(z).\end{aligned} \tag{7}$$

The pumping dynamics along SUAD trajectory follows $|\Psi(z)\rangle = \sum_{l=\pm}\eta_l\exp[l\mathrm{i}\int_0^z\Omega'(z')\mathrm{d}z'] \times |\Phi_l(z)\rangle$, where constant $\eta_\pm$ are determined by initial excitation conditions. Implementing the parametric boundary protocol from $\{\Theta(0) = 0,\ \theta(0) = 0\}$ to $\{\Theta(L) = 0,\ \theta(L) = \pi\}$ enables the topological edge-to-edge pumping $|\mathcal{L}\rangle \to |\mathcal{R}\rangle$ via the SUAD path $|\Phi_-(z)\rangle$. Accordingly, the condition $c_1 \ll c_2$ at $z = 0$ and L achieves a photonic transport from the first waveguide to the last. The SUAD scheme provides a systematic and experimentally accessible framework for realizing physically implementable shortcut to topological pumping. This constructive approach eliminates the need for complex engineering (e.g., NNN or imaginary couplings) required in other STA methods, making it particularly suitable for scalable implementations.

We reverse-engineer modulation profiles for both the coupling strengths between adjacent waveguides and waveguide propagation constants. The inter-waveguide separations precisely control the coupling strengths, while the laser writing speed governs the propagation constants[43] (Methods). Figure 1c shows theoretical comparison among the SUAD, LZ, Rabi-flopping, and conventional adiabatic schemes of topological pumping in 20 waveguides (Supplementary Notes 2–4). The pumping fidelity $\mathcal{F} \equiv |\gamma_N(z)|^2$ is calculated by solving CME with initialization $\gamma_1(0) = 1$. To achieve high-fidelity photonic transports ($\mathcal{F} > 0.95$), the LZ scheme leverages optimized nearest-neighbor coupling modulations to reduce the required sample length by an order of magnitude compared to the conventional pumping protocol. However, limited by the adiabatic criterion, the high fidelity of photonic transport under the LZ scheme is attainable only when the length of photonic chips is larger than 75 mm. The resonant Rabi-flopping scheme achieves nearly complete photonic transport to the 20th waveguide at around $L = 40$ mm, offering a pronounced advantage in device compactness compared to LZ scheme. However, this approach demands highly precise fabrication at that length due to the inherent constraint imposed by the area theorem in resonant gap-mode coupling[21,29,30]. Remarkably, the SUAD topological pumping scheme achieves high-fidelity photonic transport as long as sample lengths exceed 40 mm. For the sake of further comparison, we find that $c_{\max}L = 24.2$ ($c_{\max} = c_2$ defines the maximum inter-waveguide coupling in experiment) ensures photonic transport fidelity $\mathcal{F} > 0.9$ in an eight-waveguide system (Supplementary Note 5), showing an approximately 50% enhancement in compactness compared with the recently proposed approaches based on quantum metric with $c_{\max}L = 44.6$[26] and adiabatic infimum with $c_{\max}L = 56.8$[27].

In our SUAD topological pumping regime, as illustrated by the case of $L = 60$ mm, the propagation constants of the eigenmodes relative to β_1 are calculated (Fig. 1d), revealing a substantial spectral gap in their eigenmode spectra. Two gap modes $|\phi_\pm(z)\rangle$ are clearly separated by $2\Omega(z)$. Although there exist nonadiabatic leakages between $|\phi_\pm\rangle$ during a short-L pumping process, one of the SUAD modes, $|\Phi_-(z)\rangle$, whose mode distribution is shown in Fig. 1e, acts as a robust evolution pathway without any leakages to $|\Phi_+(z)\rangle$ under the SUAD-frame CD driving, ensuring a fast topological photonic transport. During this evolution, the accumulated geometric phase is zero (Supplementary Note 1), but the evolution can be also designed to be purely geometric when we concentrate on geometric implementation in z-direction of SUAD topological pumping by using methods of geometric quantum gates[44].

https://doi.org/10.1038/s41467-025-67693-6

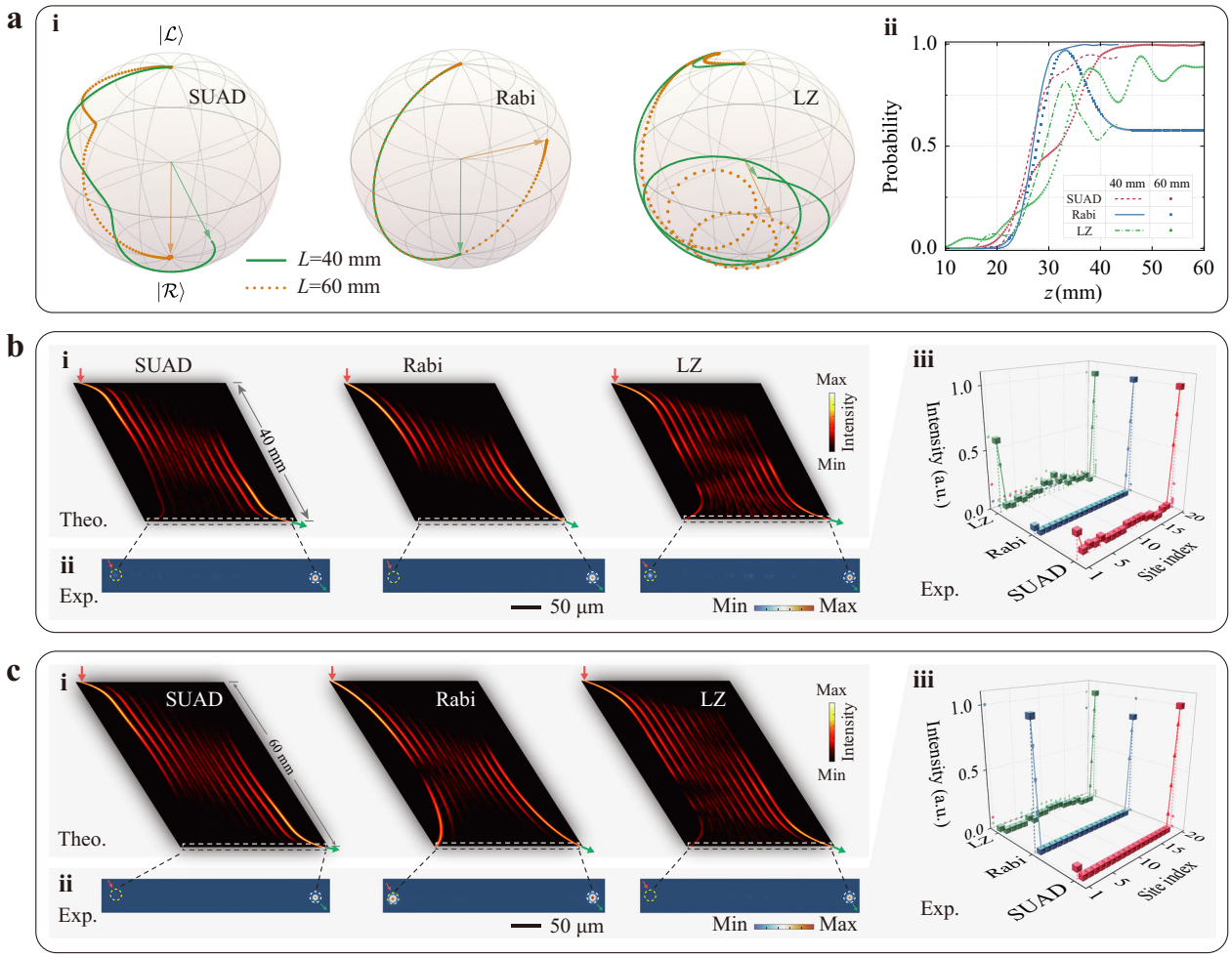

Fig. 2 | Acceleration performance of SUAD topological pumping. **a**(i) Pseudospin dynamics of edge modes $|\mathcal{L}\rangle$ and $|\mathcal{R}\rangle$ on Bloch spheres for three pumping schemes with L = 40 and 60 mm; (ii) Occupation probabilities of $|\mathcal{R}\rangle$ along the system evolution with L = 40 and 60 mm. **b**(i) Theoretically calculated light propagation; (ii) Experimentally captured intensities at the output facet; (iii) Experimental light intensity profiles of the samples with L = 40 mm for the three pumping schemes. **c** Counterpart of **b** for L = 60 mm. Data in **a**, **b**(i) and **c**(i) are obtained by solving CME with the full Hamiltonian $\widehat{H}(z)$.

Performances of topological pumping

To validate the performance of topological pumping, we fabricated two distinct sets of 20-waveguide samples with lengths of 40 mm and 60 mm, respectively. Each set comprises three samples corresponding to the SUAD, Rabi-flopping, and LZ pumping schemes. An 808 nm wavelength laser source (CNI, MDL-III-808L) was coupled into the first waveguide of each sample to serve as the input port. The light intensity distributions were recorded at the output side of the sample using a charge-coupled device (SP928, Ophir).

We visualize the pseudospin dynamics of the edge modes $|\mathcal{L}\rangle$ and $|\mathcal{R}\rangle$ as geometric trajectories on Bloch spheres, where the polar angle encodes their superposed proportion and the azimuthal angle their relative phase. Figure 2a(i) displays the trajectories of gap-mode evolution on Bloch spheres for the three pumping schemes with two different sample lengths, visually illustrating how topological pumping directs the dynamics of light between distinct edge modes. The Rabi-flopping pumping scheme achieves a pseudospin flip via a great-circle geodesic, minimizing the required length at the cost of increased sensitivity to parameters. In contrast, the LZ scheme employs a multicyclic helical traversal, which enhances robustness against local fluctuations but necessitates extended space. Notably, the SUAD pumping scheme strikes an optimized balance by maintaining robustness while achieving accelerated topological pumping. Complementing these geometric representations, Fig. 2a(ii) quantifies the pumping performance by tracking the spatial evolution of right-edge mode occupation probabilities for different sample lengths. It quantitatively highlights that the SUAD scheme achieves accelerated pumping with a reduced system length, while maintaining high pumping fidelity with independence on system lengths when exceeding a certain value (40 mm).

Experimentally, the output facet photographs and output intensity distributions for the six samples are presented in Figs. 2b(ii) (L = 40 mm) and 2c(ii) (L = 60 mm) and in Figs. 2b(iii) and 2c(iii), respectively. The measured output power distributions across the 20 waveguides agree well with the theoretical predictions in Figs. 2b(i) and 2c(i). In both length cases, the LZ scheme exhibits noticeable light diffusion into the bulk waveguides at the output, indicating inefficient topological pumping. For the Rabi-flopping pumping, effective localization in the 20th waveguide is observed only when L = 40 mm, suggesting sensitivity to length of the system. In contrast, the SUAD scheme demonstrates strong light confinement at the output of the 20th waveguide in both cases, confirming our theoretical prediction.

To highlight superior performance of the SUAD pumping over Rabi-flopping pumping, we systematically compare their tolerance of light propagation operated beyond the designed wavelength (808 nm). Finite-element simulations (FES) in Fig. 3a(i) show that the SUAD pumping maintains high fidelity ($\mathcal{F} > 0.95$) across a broad bandwidth (650–920 nm). In contrast, Rabi-flopping pumping exhibits

https://doi.org/10.1038/s41467-025-67693-6

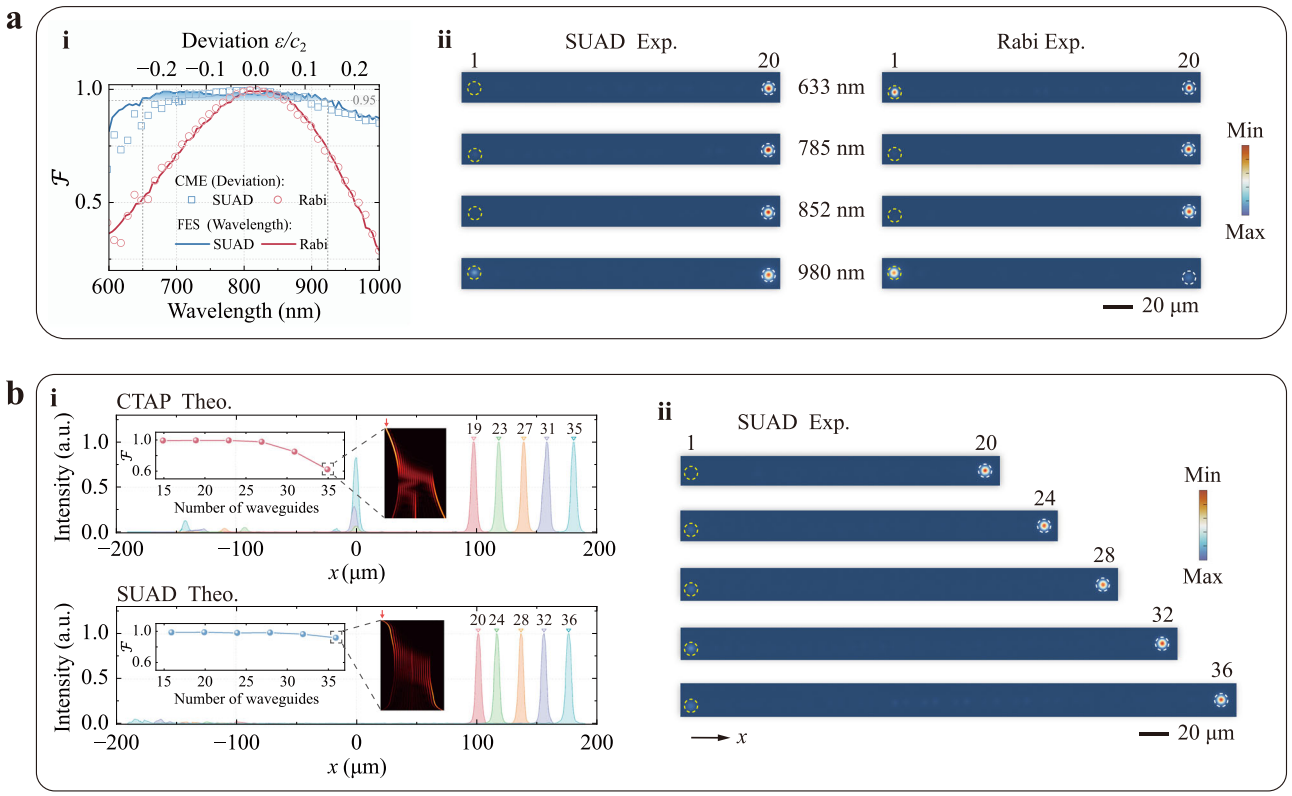

Fig. 3 | Broadband and scalable performances of SUAD topological pumping. **a**(i) Predicted pumping fidelity with input wavelength ranging from 600 to 1000 nm for SUAD (L = 60 mm, top shadow for $\mathcal{F} > 0.95$) and Rabi-flopping (L = 40 mm) schemes; (ii) Measured photographs at the end facets of the two samples working at specified four wavelengths instead of 808 nm. **b**(i) Calculated light intensity profiles at the output facet for different numbers of waveguides in CTAP (top) and SUAD (bottom) pumping schemes. Inset: Pumping fidelity trends of CTAP and SUAD schemes with different numbers of waveguides. Light propagation patterns for N = 35 (CTAP) and N = 36 (SUAD). (ii) Measured photographs at the end facets of five samples with N = 20, 24, 28, 32, and 36, respectively. $\mathcal{F}$-wavelength data in **a**(i) and intensity data in **b**(i) are obtained by FES. $\mathcal{F}$-ϵ data in **a**(i) and $\mathcal{F}$ data (inset) in **b**(i) are obtained by solving CME.

strong sensitivity to wavelength deviations due to wavelength-dependent coupling variations. To further investigate this behavior, we analyze the relationship between pumping fidelity and coupling deviation ϵ, changing $c_{1,2}$ to $c_{1,2} + \epsilon$. This analysis reveals a linear dependence between wavelength and the inter-waveguide coupling strength (Supplementary Note 6), explaining wavelength dependence of the Rabi-flopping pumping. Experimentally, we used four additional laser wavelengths (633, 785, 852, and 980 nm) and suitable sample lengths (Rabi-flopping: 40 mm; SUAD: 60 mm) to corroborate these findings. End-facet measurements in Fig. 3a(ii) show that SUAD pumping maintains robust light confinement in the 20th waveguide across the tested spectrum, while Rabi-flopping pumping fails to sustain good localization except near 808 nm, confirming SUAD pumping exhibits robust spectral performance across the operation wavelengths, whereas Rabi-flopping pumping suffers significant fidelity degradation at detuned wavelengths from 808 nm.

We finally investigate the scalability of SUAD topological pumping at L = 75 mm, for which the Rabi flopping and LZ schemes exhibit limited efficiency even for 20-waveguide configurations. To this end, we compare the SUAD scheme with the recently demonstrated interface-induced CTAP topological pumping method[24], which has theoretically shown promising scalability[23] (Supplementary Note 7). Theoretical analysis in Fig. 3b(i) reveals distinct scaling behaviors for the two schemes as the number of waveguides increases in our photonic system. Although the spectrum gap progressively becomes narrow with N (Supplementary Fig. S17), inevitably compromising topological protection, the SUAD scheme demonstrates remarkable resilience, maintaining higher fidelity compared to CTAP pumping. This enhanced scalability originates from the SUAD's accelerated pumping dynamics, which effectively mitigates finite-size effect. Experimental verification involves five SUAD samples with N ranging from 20 to 36 by interval 4. End-facet measurements of light intensity under 808 nm in Fig. 3b(ii) reveal two key findings: a well-characterized fidelity scaling law (gradual fidelity reduction with increasing N) and persistent light localization in the terminal waveguide across all configurations. These results establish SUAD pumping as a viable approach for scalable topological photonics requiring combination of robust performance and enhanced scalability, representing a significant advance over conventional pumping schemes.

Discussion

We have established a gap-mode shortcut strategy for constructing SUAD topological pumping as an efficient mechanism for spatially compressed, high-fidelity photonic transport through both theoretical investigation and on-chip experimental validation. To implement real, nearest-neighbor CD driving in the interaction picture of SUAD protocol, we have harnessed the topological protection intrinsic to the photonic waveguide system, which emerges from gap-mode pseudospin dynamics governed by an effective Hamiltonian. Our results demonstrate that SUAD topological pumping achieves a 20-fold reduction in spatial footprint compared to conventional adiabatic pumping while offering 50% greater compactness than the optimized LZ pumping as well as the recently proposed quantum metric and adiabatic infimum protocols. SUAD topological pumping achieves two critical advances for practical photonic integration: broadband operation (650–920 nm) and scalable performance in waveguide arrays.

Beyond the SSH-model implementations, the SUAD framework exhibits universal applicability across diverse classical and quantum topological platforms featuring multi-gap physics, including interfaced SSH configurations[23,24], Harper-type modulated lattices[45], flat-band non-Abelian systems in both 1D and 2D geometries[10,46,47] (Supplementary Note 8). The scalability arises from its reliance on local frame transformations rather than global diagonalization, thereby avoiding the curse of dimensionality. This feature makes SUAD particularly well suited for photonic, phononic, and quantum synthetic matter platforms where precise spatial and temporal control of system parameters is experimentally feasible. This versatility establishes SUAD topological pumping as a general strategy for accelerating complex topological dynamics across dimensions, enabling robust and fast/compact operations in chip-scale topological devices.

Methods

Sample fabrication and measurement

The optical waveguide arrays were fabricated using a femtosecond laser (CARBIDE, Light Conversion Ltd.) with a central wavelength of 1030 nm, a pulse width of 290 fs, and a repetition rate of 1 MHz. The femtosecond laser, modulated by a spatial light modulator, was focused onto a borosilicate glass sample (Eagle XG, Corning) at a depth of 170 μm using a microscope objective (40×, NA = 0.75, UPlanFLN, Olympus). The waveguide arrays were fabricated with a laser power of 210 mW. The broadband robustness testing was carried out using continuous-wave lasers with wavelengths of 633 nm (CNI, MDL-III-633L), 785 nm (CNI, MDL-II-785L), 852 nm (CNI, MDL-III-852L), and 980 nm (CNI, MDL-III-980L).

Edge modes and SUAD Hamiltonian

Under the protection regime of energy gap, the system dynamics can be described by an effective gap-mode Hamiltonian $\widehat{H}_{\mathrm{eff}}$. The effective coupling coefficient and the propagation constant difference between two gap modes are derived by, respectively

$$\begin{aligned}\mathcal{C}(z) &= \langle\mathcal{R}|\widehat{H}(z)|\mathcal{L}\rangle = \langle\mathcal{L}|\widehat{H}(z)|\mathcal{R}\rangle = c_1\chi^{N/2-1}(1-\chi^2)/(1-\chi^N),\\ \Delta\beta(z) &= \langle\mathcal{R}|\widehat{H}(z)|\mathcal{R}\rangle - \langle\mathcal{L}|\widehat{H}(z)|\mathcal{L}\rangle = \beta_2(z)-\beta_1.\end{aligned} \tag{8}$$

Expressions of the gap-mode Hamiltonian in different frames are connected by unitary transformations. Toward the AD frame, the unitary operator is $\widehat{U}_{\mathrm{AD}}(z)=\sum_{l=\pm}|\phi_l(z)\rangle\langle\phi_l|$, where z-independent $|\phi_\pm\rangle$ are basis vectors in the adiabatic frame. Then we can derive

$$\begin{aligned}\widehat{H}_{\mathrm{AD}}(z) &= \widehat{U}^{\dagger}_{\mathrm{AD}}(z)\widehat{H}_{\mathrm{eff}}\widehat{U}_{\mathrm{AD}}(z) + \mathrm{i}\widehat{U}^{\dagger}_{\mathrm{AD}}(z)\partial_z\widehat{U}_{\mathrm{AD}}(z)\\ &= \Omega(z)\sum_{l=\pm} l|\phi_l\rangle\langle\phi_l| - \mathrm{i}\partial_z\theta(z)\left(|\phi_+\rangle\langle\phi_-| - |\phi_-\rangle\langle\phi_+|\right)/2.\end{aligned} \tag{9}$$

Through a similar process, the Hamiltonian in the SUAD frame is

$$\begin{aligned}\widehat{H}_{\mathrm{SUAD}}(z) &= \widehat{U}^{\dagger}_{\mathrm{SUAD}}(z)\widehat{H}_{\mathrm{AD}}\widehat{U}_{\mathrm{SUAD}}(z) + \mathrm{i}\widehat{U}^{\dagger}_{\mathrm{SUAD}}(z)\partial_z\widehat{U}_{\mathrm{SUAD}}(z)\\ &= \Omega'(z)\sum_{l=\pm} l|\Phi_l\rangle\langle\Phi_l| - \partial_z\Theta(z)\left(|\Phi_+\rangle\langle\Phi_-| + |\Phi_-\rangle\langle\Phi_+|\right)/2,\end{aligned} \tag{10}$$

for which the unitary operator is defined by $\widehat{U}_{\mathrm{SUAD}}(z)=\sum_{l=\pm}|\Phi_l(z)\rangle\langle\Phi_l|$, with $|\Phi_\pm\rangle$ being z-independent basis vectors in the SUAD frame. To eliminate the nonadiabatic leakage (the second term in $\widehat{H}_{\mathrm{SUAD}}$), the SUAD CD driving should be $\widehat{h}_{\mathrm{CD}} = \sin\theta(z)\partial_z\Theta(z)(|L\rangle\langle L| - |R\rangle\langle R|)/2 + \cos\theta(z)\partial_z\Theta(z)(|L\rangle\langle R| + |R\rangle\langle L|)/2$. In the gap-mode frame, the effective modulation parameters are supposed to be modified as

$$\begin{aligned}\mathcal{C}'(z) &= \mathcal{C}(z) + \partial_z\Theta(z)\cos\theta(z)/2,\\ \Delta\beta'(z) &= \Delta\beta(z) - \partial_z\Theta(z)\sin\theta(z),\end{aligned} \tag{11}$$

corresponding to Eq. (7).

Modulation of coupling coefficients and propagation constants

Waveguide arrays with specific coupling coefficients and propagation constants were fabricated by controlling the coupling separation (the center-to-center distance between adjacent waveguides, minimum 6 μm and maximum 15 μm) and scanning speed (see Supplementary Notes 9 and 10 for more details), respectively. The Rabi-flopping samples were fabricated with a scanning speed of 40 mm/s, with the coupling coefficients modulated by controlling the waveguide coupling separation. For other samples, a variable scanning speed strategy was employed to construct waveguide arrays with tunable propagation constants.

Data availability

The raw data that support the findings of this study are available from the corresponding author upon reasonable request.

Code availability

The codes used in this paper are available from the corresponding authors upon request.

References

1. Lu, L., Joannopoulos, J. D. & Soljačić, M. Topological photonics. *Nat. Photon.* **8**, 821–829 (2014).
2. Noh, J. et al. Topological protection of photonic mid-gap defect modes. *Nat. Photon.* **12**, 408–415 (2018).
3. Ozawa, T. et al. Topological photonics. *Rev. Mod. Phys.* **91**, 015006 (2019).
4. Ni, X., Yves, S., Krasnok, A. & Alù, A. Topological metamaterials. *Chem. Rev.* **123**, 7585–7654 (2023).
5. Liu, G.-G. et al. Photonic axion insulator. *Science* **387**, 162–166 (2025).
6. Kraus, Y. E., Lahini, Y., Ringel, Z., Verbin, M. & Zilberberg, O. Topological states and adiabatic pumping in quasicrystals. *Phys. Rev. Lett.* **109**, 106402 (2012).
7. Lohse, M., Schweizer, C., Price, H. M., Zilberberg, O. & Bloch, I. Exploring 4D quantum Hall physics with a 2D topological charge pump. *Nature* **553**, 55–58 (2018).
8. Zilberberg, O. et al. Photonic topological boundary pumping as a probe of 4D quantum Hall physics. *Nature* **553**, 59–62 (2018).
9. Jürgensen, M., Mukherjee, S. & Rechtsman, M. C. Quantized nonlinear Thouless pumping. *Nature* **596**, 63–67 (2021).
10. Sun, Y. K. et al. Non-Abelian Thouless pumping in photonic waveguides. *Nat. Phys.* **18**, 1080–1085 (2022).
11. Cheng, Q. et al. Asymmetric topological pumping in nonparaxial photonics. *Nat. Commun.* **13**, 249 (2022).
12. Citro, R. & Aidelsburger, M. Thouless pumping and topology. *Nat. Rev. Phys.* **5**, 87–101 (2023).
13. Walter, A. S. et al. Quantization and its breakdown in a Hubbard-Thouless pump. *Nat. Phys.* **19**, 1471–1475 (2023).
14. Szameit, A. & Rechtsman, M. C. Discrete nonlinear topological photonics. *Nat. Phys.* **20**, 905–912 (2024).
15. Wang, J., Li, K. & Quan, Z. Integrated structured light manipulation. *Photon. Insights* **3**, R05 (2024).
16. Gao, J., Xu, Z. S., Yang, Z., Zwiller, V. & Elshaari, A. W. Quantum topological photonics with special focus on waveguide systems. *npj Nanophoton.* **1**, 34 (2024).
17. Yan, W., Zhang, B. & Chen, F. Photonic topological insulators in femtosecond laser direct-written waveguides. *npj Nanophoton.* **1**, 40 (2024).
18. Garanovich, I. L., Longhi, S., Sukhorukov, A. A. & Kivshar, Y. S. Light propagation and localization in modulated photonic lattices and waveguides. *Phys. Rep.* **518**, 1–79 (2012).

19. Menchon-Enrich, R. et al. Spatial adiabatic passage: a review of recent progress. *Rep. Prog. Phys.* **79**, 074401 (2016).
20. Privitera, L., Russomanno, A., Citro, R. & Santoro, G. E. Nonadiabatic breaking of topological pumping. *Phys. Rev. Lett.* **120**, 106601 (2018).
21. Longhi, S., Giorgi, G. L. & Zambrini, R. Landau-Zener topological quantum state transfer. *Adv. Quantum Technol.* **2**, 1800090 (2019).
22. Poli, C., Bellec, M., Kuhl, U., Mortessagne, F. & Schomerus, H. Selective enhancement of topologically induced interface states in a dielectric resonator chain. *Nat. Commun.* **6**, 6710 (2015).
23. Longhi, S. Topological pumping of edge states via adiabatic passage. *Phys. Rev. B* **99**, 155150 (2019).
24. Tian, T. et al. Experimental realization of nonreciprocal adiabatic transfer of phonons in a dynamically modulated nanomechanical topological insulator. *Phys. Rev. Lett.* **129**, 215901 (2022).
25. Deng, J. et al. Observing the quantum topology of light. *Science* **378**, 966–971 (2022).
26. Song, W. et al. Fast topological pumps via quantum metric engineering on photonic chips. *Sci. Adv.* **10**, eadn5028 (2024).
27. Wu, S. et al. Approaching the adiabatic infimum of topological pumps on thin-film lithium niobate waveguides. *Nat. Commun.* **15**, 9805 (2024).
28. Hu, S., Li, S., Hu, M. & Lei, Z. Symmetry-protected Landau-Zener-Stückelberg-Majorana interference and nonadiabatic topological transport of edge states. *Phys. Rev. A* **111**, 052414 (2025).
29. Lang, N. & Büchler, H. P. Topological networks for quantum communication between distant qubits. *npj Quantum Inf.* **3**, 47 (2017).
30. Hu, S., Hu, M., Li, S., Zhong, Z. & Lei, Z. Hong-Ou-Mandel interference in a temporal-average-inversion-symmetric chain. *Phys. Rev. A* **110**, 032438 (2024).
31. D'Angelis, F. M., Pinheiro, F. A., Guéry-Odelin, D., Longhi, S. & Impens, F. Fast and robust quantum state transfer in a topological Su-Schrieffer-Heeger chain with next-to-nearest-neighbor interactions. *Phys. Rev. Res.* **2**, 033475 (2020).
32. Guo, J. K., Wu, J. L., Cao, J., Zhang, S. & Su, S. L. Shortcut engineering for accelerating topological quantum state transfers in optomechanical lattices. *Phys. Rev. A* **110**, 043510 (2024).
33. Romero, S. V., Chen, X., Platero, G. & Ban, Y. Optimizing edge-state transfer in a Su-Schrieffer-Heeger chain via hybrid analog-digital strategies. *Phys. Rev. Appl.* **21**, 034033 (2024).
34. Liu, W., Ke, Y. & Lee, C. Shortcuts to adiabatic topological pumping. *Phys. Rev. A* **112**, 013317 (2025).
35. Guéry-Odelin, D. et al. Shortcuts to adiabaticity: concepts, methods and applications. *Rev. Mod. Phys.* **91**, 045001 (2019).
36. Zhang, X. L. et al. Non-Abelian braiding on photonic chips. *Nat. Photon.* **16**, 390–395 (2022).
37. Song, W. et al. Shortcuts to adiabatic non-Abelian braiding on silicon photonic chips. *Sci. Adv.* **11**, eadt7224 (2025).
38. Berry, M. V. Quantum phase corrections from adiabatic iteration. *Proc. R. Soc. Lond. A* **414**, 3–46 (1987).
39. Ibáñez, S., Chen, X., Torrontegui, E., Muga, J. G. & Ruschhaupt, A. Multiple Schrödinger pictures and dynamics in shortcuts to adiabaticity. *Phys. Rev. Lett.* **109**, 100403 (2012).
40. Baksic, A., Ribeiro, H. & Clerk, A. A. Speeding up adiabatic quantum state transfer by using dressed states. *Phys. Rev. Lett.* **116**, 230503 (2016).
41. Wu, J. L., Su, S. L., Ji, X. & Zhang, S. Superadiabatic scheme for optimizing the fast generation of tree-type 3D entanglement. *Ann. Phys.* **386**, 34–43 (2017).
42. Zhou, B. et al. Accelerated quantum control using superadiabatic dynamics in a solid-state lambda system. *Nat. Phys.* **13**, 330–334 (2017).
43. Yu, F. et al. Resetting directional couplers for high-fidelity quantum photonic integrated chips. *Opt. Lett.* **46**, 5181–5184 (2021).
44. Wu, J. L. & Su, S. L. Universal speeded-up adiabatic geometric quantum computation in three-level systems via counterdiabatic driving. *J. Phys. A* **52**, 335301 (2019).
45. Chen, Z. G., Tang, W., Zhang, R. Y., Chen, Z. & Ma, G. Landau-Zener transition in the dynamic transfer of acoustic topological states. *Phys. Rev. Lett.* **126**, 054301 (2021).
46. You, O. et al. Observation of non-Abelian Thouless pump. *Phys. Rev. Lett.* **128**, 244302 (2022).
47. Sun, Y. K., Shan, Z. L., Tian, Z. N., Chen, Q. D. & Zhang, X. L. Two-dimensional non-Abelian Thouless pump. *Nat. Commun.* **15**, 9311 (2024).

Acknowledgements

This work was supported by the National Natural Science Foundation of China (Grants No. 62571494 J.-L.W., No. 12304407 J.-L.W., No. 12274376 S.-L.S., No. 12205256 Y.W., No. 62375103 Z.-N.T., and No. 12474396 X.N.), the Natural Science Foundation of Henan Province (Grants No. 232300421075 S.-L.S.), and the China Postdoctoral Science Foundation (Grants No. 2023TQ0310 J.-L.W. and No. 2024M762973 J.-L.W.). K.-H.X. thanks X. Yang and W.-Z. Fan for their assistance with the sample fabrication and measurement.

Author contributions

J.-L.W., K.-H.X., X.N., S.-L.S., and Z.-N.T. conceived the concept and scheme for the SUAD topological pumping. J.-L.W. and X.N. performed the theoretical analysis and designed the experiment. K.-H.X. and Z.-Z.L. fabricated the samples and carried out the experimental measurements under the supervision of Z.-N.T. and Q.-D.C. Data analysis was assisted by J.-K.G., Y.W., and X.-L.Z. The manuscript was written by J.-L.W., K.-H.X., and X.N. with input from all authors. All authors reviewed and commented on the manuscript. The project was supervised by Q.-D.C. and H.-B.S.

Competing interests

The authors declare no competing interests.

Additional information

Supplementary information The online version contains supplementary material available at https://doi.org/10.1038/s41467-025-67693-6.

Correspondence and requests for materials should be addressed to Shi-Lei Su, Zhen-Nan Tian or Hong-Bo Sun.

Peer review information *Nature Communications* thanks Zhoutao Lei, Tao Li, and the other, anonymous, reviewer(s) for their contribution to the peer review of this work. A peer review file is available.